Spectroscopic and Theoretical Study of Endohedral Dimetallofullerene Having a Non-IPR Fullerene Cage: $Ce_2@C_{72}$

Michio Yamada,[†] Takatsugu Wakahara,[†] Takahiro Tsuchiya,[†] Yutaka Maeda,[‡] Takeshi Akasaka,*[,†] Naomi Mizorogi,[§] and Shigeru Nagase*[,§]

Center for Tsukuba Advanced Research Alliance, University of Tsukuba, Tsukuba, Ibaraki 305-8577, Japan, Department of Chemistry, Tokyo Gakugei University, Koganei, Tokyo 184-8501, Japan, and Department of Theoretical and Computational Molecular Science, Institute for Molecular Science, Okazaki, Aichi 444-8585, Japan

Received: October 27, 2007; Revised Manuscript Received: June 3, 2008

The endohedral dimetallofullerene having a non-IPR fullerene cage, $Ce_2@C_{72}$, is spectroscopically and theoretically characterized. The ^{13}C NMR measurements display large temperature-dependent signals caused by paramagnetic shifts, indicating that the Ce atoms are located near the two fused pentagons in the C_{72} cage. Theoretical calculations are performed to clarify the metal position, which are in good agreement with the result obtained by the paramagnetic ^{13}C NMR analysis. Electrochemical measurements reveal that $Ce_2@C_{72}$ has particularly lower oxidation and higher reduction potentials than other endohedral dimetallofullerenes.

Introduction

Endohedral metallofullerenes[1] have attracted much attention during the past decade not only for their unique structures but also for electronic properties because of the electron transfer from the metal atoms to the fullerene cage. For example, a representative endohedral dimetallofullerene, $La_2@C_{80}$, is a stronger electron acceptor than monometallofullerenes such as $La@C_{82}(C_{2v})$ and $La@C_{82}(C_s)$ isomers and has a remarkably smaller HOMO−LUMO gap than that for empty fullerenes.[2] Furthermore, fullerene cages that do not obey the isolated-pentagon rule (IPR)[3] have been stabilized and isolated by encapsulating metal atoms, as seen for $Sc_2@C_{66}$,[4–6] $Sc_3N@C_{68}$,[7–9] $Tb_3N@C_{84}$,[10] $Sc_2C_2@C_{68}$,[11] and $Sc_3N@C_{70}$.[12] A small lanthanide dimetallofullerene, $La_2@C_{72}$, was prepared and isolated in 1998.[13] In 2003, Shinohara and co-workers investigated its structure by observing the ^{13}C NMR spectrum.[14] The observation of 18 ^{13}C NMR lines can be satisfied with the 24 isomers of C_{72} with D_2 symmetry. If the C_{72} cage is allowed to have two fused pentagons, as in the case of $Sc_2@C_{66}$,[4–6] two non-IPR structures (#10611 and #10958) are also possible for $La_2@C_{72}$. Thus, it has been proposed that $La_2@C_{72}$ has the non-IPR D_2-C_{72} (#10611) cage on the basis of the HOMO−LUMO gap estimated from the UV−vis−NIR absorption spectrum. Recent calculations show that the C_{72}^{6-} isomer (#10611) has the lowest energy among the 39 C_{72} hexaanions including 24 D_2-C_{72} cages and 15 higher symmetry C_{72} cages (five D_{2d}, five D_{2h}, three D_3, one D_6, and one D_{6d} cage) that may lead to D_2 symmetry upon the encapsulation of two La atoms.[15] This confirms that $La_2@C_{72}$ with the non-IPR D_2 cage (#10611) is energetically the most stable (most abundantly produced), since the electronic structure is expected to be formally described as $La_2^{6+}C_{72}^{6-}$. However, the dynamic behavior of metal atoms encapsulated in the non-IPR C_{72} cage has not been elucidated yet. In this context, we have recently developed a new method to characterize the dynamic behavior of the metal atoms in paramagnetic endohedral metallofullerenes having f electrons.[16]

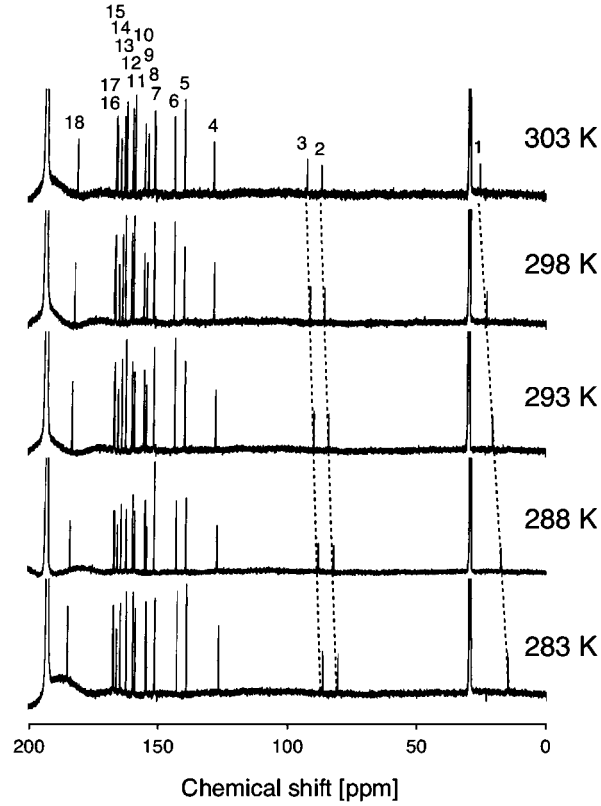

Figure 1. ^{13}C NMR spectra of $Ce_2@C_{72}$ at 283−303 K in CS_2 solution. The measured chemical shifts (ppm) at 303 K are 25.64, 86.88, 92.33, 128.31, 139.59, 143.54, 150.89, 151.21, 153.51, 154.85, 158.77, 159.61, 161.97, 162.66, 164.03, 164.03, 165.50, 165.83, and 180.76.

We herein report the ^{13}C NMR paramagnetic shift analysis and theoretical study of $Ce_2@C_{72}$ having a non-IPR fullerene cage. Its unique redox property is also investigated by means of electrochemical measurements.

* Corresponding author. E-mail: akasaka@tara.tsukuba.ac.jp.
[†] University of Tsukuba.
[‡] Tokyo Gakugei University.
[§] Institute for Molecular Science.

10.1021/jp804260d CCC: $40.75
Published on Web 07/31/2008

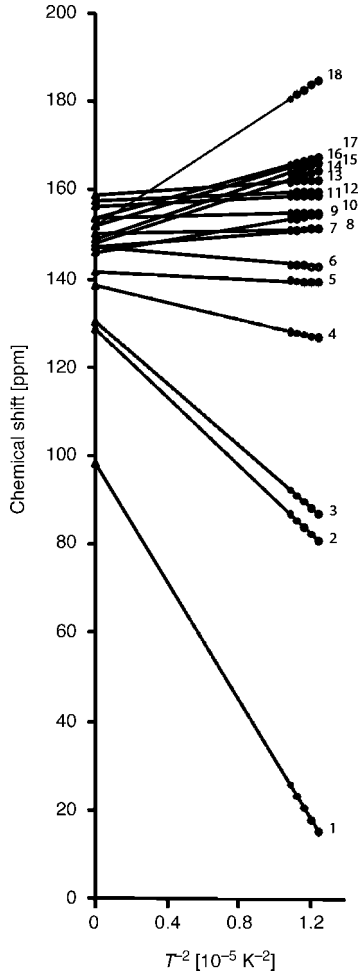

Figure 2. Line fitting plot for all carbon atoms of $Ce_2@C_{72}$; chemical shift vs T^{-2}. Observed chemical shifts (●) and extrapolated values (▲) at $T^{-2} = 0$ on the line fitting.

Experimental Section

Preparation and Purification of $Ce_2@C_{72}$. $Ce_2@C_{72}$ was prepared and purified according to a reported method.[17] Briefly, the soot containing cerium metallofullerenes was prepared using a composite anode which contains graphite and cerium oxide with the atomic ratio of Ce/C equal to 2.0%. The composite rod was subjected to an arc discharge as an anode under a 150 Torr He pressure. The raw soot containing cerium metallofullerenes was collected and extracted with *N*,*N*-dimethylformamide (DMF) solvent for 15 h. The soluble fraction was injected into the HPLC; a Buckyprep column (20 mm × 250 mm i.d.; Cosmosil, Nacalai Tesque, Inc.) was used to afford the pure $Ce_2@C_{72}$. Electrochemical grade tetra-*n*-butylammonium perchlorate (TBAP), purchased from Wako, was recrystallized from absolute ethanol and dried under vacuum at 313 K prior to use. 1,2-Dichlorobenzene (ODCB) was distilled over P_2O_5 under vacuum prior to use. Mass spectroscopy was performed on a Bruker BIFLEX III. The UV−Vis−NIR absorption spectrum was measured with a Shimadzu UV-3150 spectrometer. Cyclic voltammetry (CV) and differential pulse voltammetry (DPV) in ODCB were carried out using a BAS CW-50. A conventional three-electrode cell used for CV and DPV measurements consists of a platinum working electrode, a platinum counter electrode, and a saturated calomel reference electrode (SCE). All potentials are referenced to the ferrocene/ferrocenium couple (Fc/Fc^+) as the standard. CV: scan rate, 20 mV s^{-1}. DPV: Pulse amplitude, 50 mV; pulse width, 50 ms; pulse period, 200 ms; scan rate, 20 mV s^{-1}. NMR spectra were obtained with a Bruker AVANCE-500 with a CryoProbe system. The ^{13}C NMR chemical shifts were calibrated with CS_2 as an internal reference (δ 195.0).

Theoretical Calculations. Geometry optimization was carried out at the Hartree−Fock (HF) level using the Gaussian 03 program.[18] The relativistic effective core potential (ECP) and CEP-31G[19] basis set were used for Ce. The split-valence d-polarized 6−31G(d)[20] basis set was used for C.

Results and Discussion

The ^{13}C NMR spectrum of $Ce_2@C_{72}$ in CS_2 shows 18 lines, as shown in Figure 1. The peak heights of carbon signals numbered 1, 2, and 3 are lower than those of other lines. However, the line widths of these three signals are larger than the others, indicating the presence of 18 lines with equal intensity. This result reveals that $Ce_2@C_{72}$ has D_2 symmetry, as does $La_2@C_{72}$.[14] Interestingly, the three broad carbon signals numbered 1, 2, and 3 are in higher magnetic field region: 25.64 (No.1), 86.88 (No. 2), and 92.33 (No. 3) ppm at 303 K. In addition, these signals are highly broadened by the stronger

TABLE 1: Data Table for Figure 2

carbon number	extrapolated value (δ_{dia} [ppm] at $T^{-2} = 0$)	chemical shift (ppm) at 303 K	at 298 K	at 293 K	at 288 K	at 283 K	square of the correlation coefficient
1	98.4	25.6	23.1	20.4	17.7	15.0	0.9996
2	128.6	86.9	85.4	83.9	82.3	80.8	0.9996
3	130.4	92.3	91.0	89.6	88.2	86.8	0.9996
4	138.7	128.3	128.0	127.6	127.1	126.8	0.9932
5	141.9	139.6	139.5	139.4	139.3	139.2	0.9995
6	147.6	143.5	143.4	143.2	143.1	142.9	0.9994
7	147.3	150.9	151.0	151.2	151.3	151.4	0.9981
8	150.4	151.2	151.2	151.3	151.3	151.3	0.9993
9	146.2	153.5	153.8	154.0	154.3	154.6	0.9993
10	154.0	154.9	154.9	154.9	155.0	155.0	0.9841
11	156.7	158.8	158.8	158.9	159.0	159.1	0.9987
12	157.7	159.6	159.7	159.8	159.8	159.9	0.9959
13	159.1	162.0	162.1	162.2	162.3	162.4	0.9991
14	148.2	162.7	163.2	163.7	164.2	164.8	0.9996
15	149.0	164.0	164.6	165.1	165.7	166.2	0.9996
16	152.2	165.5	166.0	166.4	166.9	167.4	0.9996
17	153.9	165.8	166.3	166.7	167.1	167.6	0.9996
18	152.1	180.8	181.8	182.8	183.9	184.9	0.9997

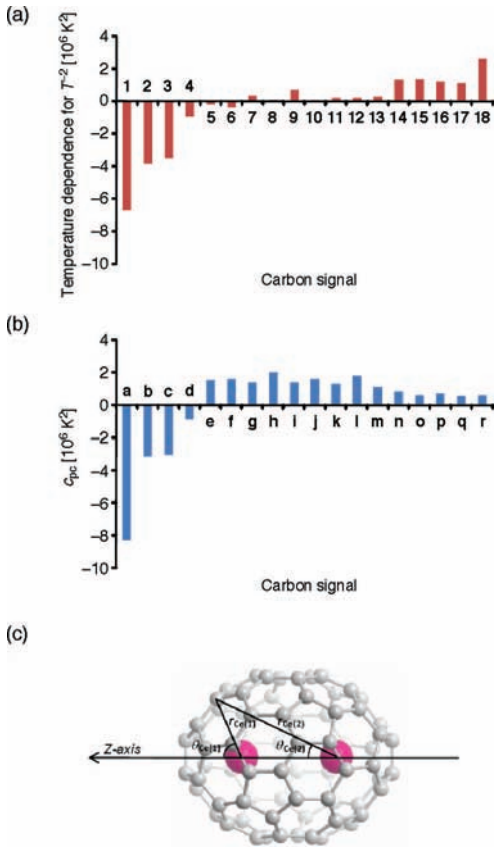

Figure 3. (a) The observed temperature dependence for T^{-2} and (b) the calculated c_{pc} values for the carbon signals of $Ce_2@C_{72}$. (c) The definition of $r_{Ce(1)}$, $r_{Ce(2)}$, $\theta_{Ce(1)}$, and $\theta_{Ce(2)}$ for $Ce_2@C_{72}$.

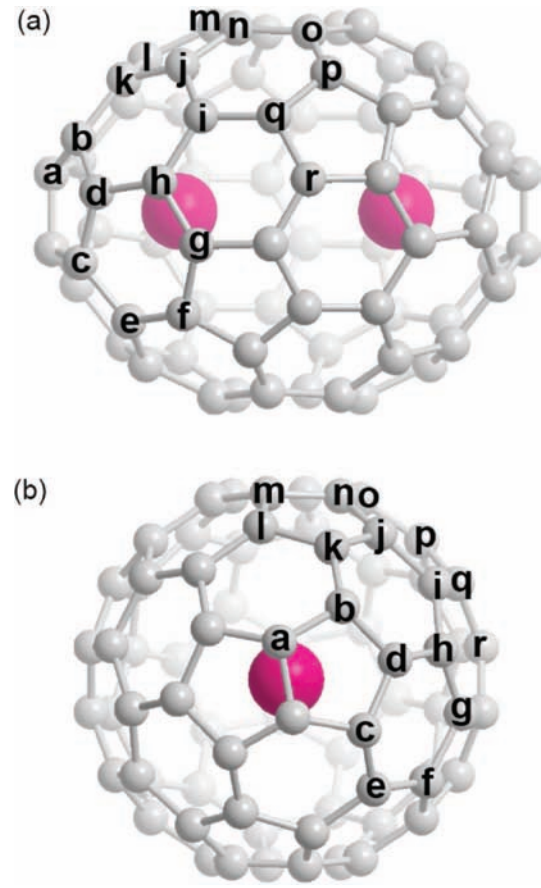

Figure 4. (a) Front and (b) side views of the optimized structure of D_2-$Ce_2@C_{72}$ (#10611).

paramagnetic effects. It has been reported that the ^{13}C NMR signals of $Ce_2@C_{80}$ show small temperature dependence since the Ce atoms move around inside the C_{80} cage.[21] In contrast, all the carbon signals of $Ce_2@C_{72}$ exhibit larger temperature-dependent shifts that originate from the f-electron spin remaining on the Ce^{3+} ($4f^15d^06s^2$) cation. This indicates that the Ce atoms in $Ce_2@C_{72}$ do not move around but rather stand still inside the C_{72} cage. The chemical shifts of paramagnetic molecules in solutions are generally expressed as a sum of three contributions from diamagnetic (δ_{dia}), Fermi contact (δ_{fc}), and pseudocontact (δ_{pc}) shifts (eq 1) where the paramagnetic δ_{fc} and δ_{pc} are proportional to T^{-1} and T^{-2} (T = absolute temperature), respectively.[22] Constants c_{fc} and c_{pc} in eq 1 are characteristic values of individual carbon signals.

$$\delta = \delta_{dia} + \delta_{fc} + \delta_{pc} = \delta_{dia} + \frac{c_{fc}}{T} + \frac{c_{pc}}{T^2} \quad (1)$$

For cerium metallofullerenes, it has been clarified that δ_{pc} makes a much larger contribution than δ_{fc}, as is apparent from the fact that there is no significant connection between the Ce atoms and cage carbons.[16,23] Therefore, the observed temperature-dependent shifts of $Ce_2@C_{72}$ are mostly derived from the pseudocontact interaction. Figure 2 shows the line fitting plots for all carbon chemical shifts of $Ce_2@C_{72}$ as a function of T^{-2}. The chemical shifts are listed in Table 1.

Figure 2 and Table 1 clearly show that there are good linear correlations between chemical shifts and T^{-2} for all carbon signals. The extrapolated values at $T^{-2} = 0$ in the plot of Figure 2 correspond to the δ_{dia} of the corresponding carbons, as indicated by eq 1. The δ_{dia} values range from 100 to 160 ppm. This region agrees well with that of 130−160 ppm for the chemical shifts of $La_2@C_{72}$.[14] This agreement clearly confirms that the δ_{dia} of $Ce_2@C_{72}$ corresponds to the chemical shifts of $La_2@C_{72}$, and Fermi contact interaction can be ignored. Therefore, the chemical shifts of $Ce_2@C_{72}$ are briefly expressed as eq 2. In eq 2, r is the distance between Ce and cage carbons, θ is the angle between the r vector and the vertical axis on which the two Ce atoms locate, and C is a common constant for all cage carbons. We have already found that C is -6.827×10^7, from the 2D-INADEQUATE NMR study of the $Ce@C_{82}$ anion.[16] The essential assumption in the paramagnetic NMR spectral analysis is that the pseudocontact shifts are produced by a sum of the individual contributions from the two Ce atoms named Ce(1) and Ce(2).

$$\delta = \delta_{dia} + \delta_{pc} = \delta_{dia} + \sum_{i=Ce(1),Ce(2)} \frac{C(3\cos^2\theta_i - 1)}{r_i^3}\frac{1}{T^2} \quad (2)$$

$$c_{pc} = \sum_{i=Ce(1),Ce(2)} \frac{C(3\cos^2\theta_i - 1)}{r_i^3} \quad (3)$$

Since eq 2 includes geometrical information (r and θ) of the encapsulated Ce atoms, we compared the observed temperature dependence of the carbon signals with the calculated values using the optimized structure of $Ce_2@C_{72}$. Figure 3a shows the observed T^{-2} dependence of δ_{pc} for the carbon signals of $Ce_2@C_{72}$, which corresponds to each slope in the plot of Figure 2. Figure 3b shows the T^{-2} dependence (c_{pc}) calculated from eqs 2 and 3, by using $C = -6.827 \times 10^{7}$[16] and the optimized structure of D_2-$Ce_2@C_{72}$ (#10611). Figure 3c shows the definition of r and θ for $Ce_2@C_{72}$. Two views of the optimized structure of $Ce_2@C_{72}$ are shown in Figure 4. It is notable that

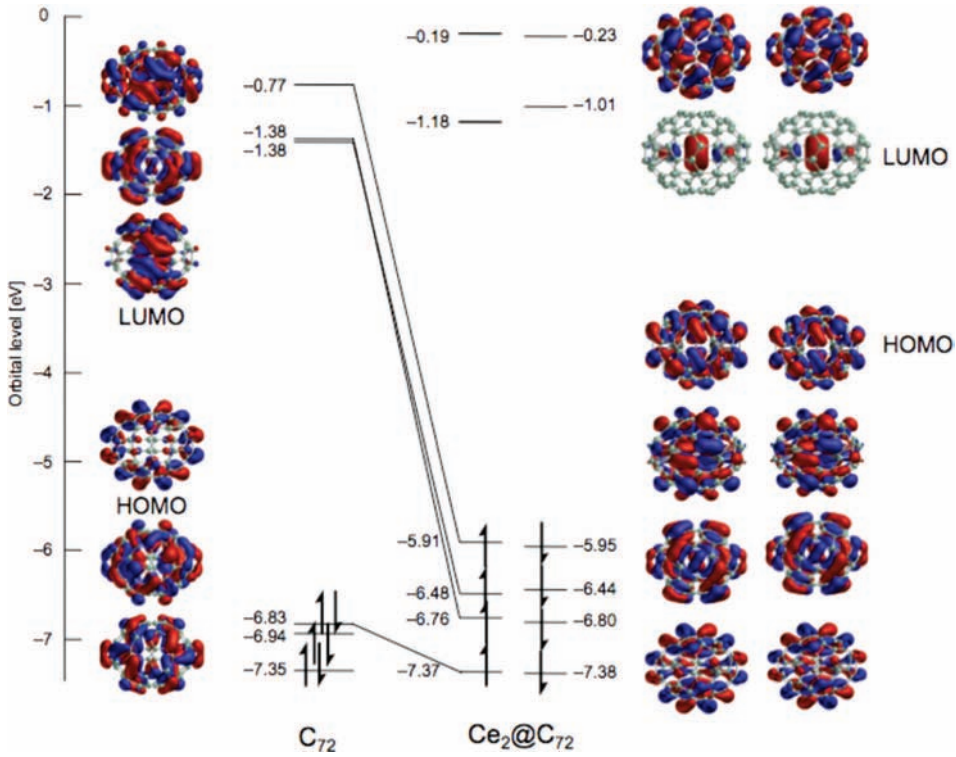

Figure 5. Molecular orbital (MO) diagrams of D_2-C_{72} (#10611) and D_2-$Ce_2@C_{72}$ (#10611).

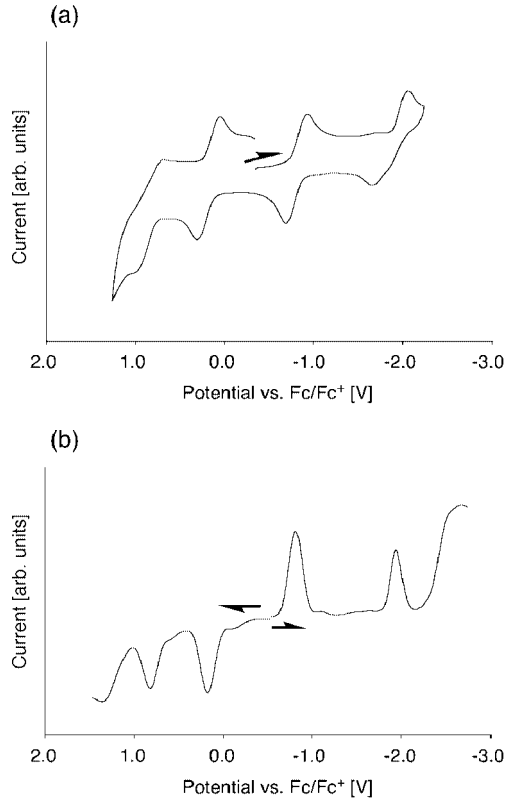

Figure 6. (a) CV and (b) DPV of $Ce_2@C_{72}$ in 1,2-dichlorobenzene containing 0.1 M $(n\text{-Bu})_4NPF_6$.

the observed values are in good agreement with the calculated values. The NMR lines named 1, 2, 3, and 4 are clearly assignable to carbons a, b (or c), c (or b), and d, respectively, as shown in Figure 4. Therefore it is concluded that the two Ce atoms are tightly located near the two-fused pentagons in the D_2-C_{72} cage, as in the optimized structure (Figure 4).

TABLE 2: Redox Potentials of $Ce_2@C_{72}$ and $Ce_2@C_{80}$[a]

compd	$^{ox}E_2$	$^{ox}E_1$	$^{red}E_1$	$^{red}E_2$
$Ce_2@C_{72}$	0.82[b,c]	0.18	−0.81	−1.86
$Ce_2@C_{80}$[d]	0.95	0.57	−0.39	−1.71

[a] Half-cell potentials unless otherwise stated. Values are in volts relative to ferrocene/ferrocenium couple. [b] Values are obtained by DPV. [c] Irreversible. [d] Reference 21.

Figure 5 shows the molecular orbital (MO) diagrams of calculated at the HF level for C_{72} and $Ce_2@C_{72}$. A total of six valence electrons are transferred from two Ce ($4f^15d^16s^2$) atoms to the C_{72} cage to occupy the LUMO, LUMO+1, and LUMO+2 of C_{72}. The α- and β-spin MO levels of $Ce_2@C_{72}$ are split by the existence of one f electron on each Ce atom. The HOMO of $Ce_2@C_{72}$ is delocalized not only on the two Ce^{3+} cations but also on the C_{72} cage. In contrast, the LUMO of $Ce_2@C_{72}$ is localized onto the two Ce^{3+} cations, as found for $La_2@C_{80}$.[24] The HOMO−LUMO gap of $Ce_2@C_{72}$ is smaller than that of C_{72}. This confirms that encapsulation of metal atoms changes the electronic structure of the non-IPR C_{72} cage.

The electronic property of $Ce_2@C_{72}$ was investigated by cyclic (CV) and differential pulse voltammetry (DPV) measurements, as shown in Figure 6. Two reversible reduction, one reversible oxidation, and two irreversible oxidation potentials were observed. The reversibility at the first oxidation as well as the first and second reduction is consistent with the fact that the $Ce_2@C_{72}$ molecule is fairly stable under ambient conditions, despite its non-IPR structure. As is apparent from the redox potentials summarized in Table 2, $Ce_2@C_{72}$ has much lower oxidation and higher reduction potentials than $Ce_2@C_{80}$.[21] The HOMO−LUMO gap of $Ce_2@C_{72}$ is larger than those of previously reported endohedral dimetallofullerenes, such as $La_2@C_{80}$.[2] These results are consistent with the theoretical calculations.

The difference between the first oxidation and the first reduction potentials of $Ce_2@C_{72}$ is 990 mV. A very similar value

(960 mV) has been also obtained for $Ce_2@C_{80}$.[21] In the related work, Shinohara and co-workers have reported the scanning tunneling spectroscopy (STS) study to characterize the electronic properties of $La_2@C_{72}$ and $La_2@C_{80}$ in multilayer islands grown on a hydrogen-terminated Si(100)-2 × 1 surface, in which the HOMO−LUMO gaps of the $La_2@C_{72}$ and $La_2@C_{80}$ multilayer are evaluated to be 1.0−1.2 and 1.3−1.5 eV, respectively.[25]

Conclusions

^{13}C NMR measurements confirm that $Ce_2@C_{72}$ has D_2 symmetry, as in the case of $La_2@C_{72}$. The four ^{13}C NMR signals associated with two fused pentagons are clearly assigned by means of the paramagnetic ^{13}C NMR shift analysis. It is also clarified that the two encapsulated Ce atoms are located near the two fused pentagons in the D_2-C_{72} cage. Theoretical calculations reveal the electronic structure of $Ce_2@C_{72}$. Electrochemical measurements indicate that $Ce_2@C_{72}$ has much lower oxidation and higher reduction potentials than $Ce_2@C_{80}$.

Acknowledgment. This work was supported in part by a Grant-in-Aid, the 21st Century COE Program, Nanotechnology Support Project, The Next Generation Super Computing Project (Nanoscience Project), and Scientific Research on Priority Area from the Ministry of Education, Culture, Sports, Science, and Technology of Japan, and a grant from the Kurata Memorial Hitachi Science and Technology Foundation.

References and Notes

(1) *Endofullerenes: A New Family of Carbon Clusters*; Akasaka, T.; Nagase, S.; Eds.; Kluwer: Dordrecht, The Netherlands, 2002.

(2) Suzuki, T.; Maruyama, Y.; Kato, T.; Kikuchi, K.; Nakao, Y.; Achiba, Y.; Kobayashi, K.; Nagase, S. *Angew. Chem., Int. Ed.* **1995**, *34*, 1094–1096.

(3) Kroto, H. W. *Nature* **1987**, *329*, 529–531.

(4) Wang, C.-R.; Kai, T.; Tomiyama, T.; Yoshida, T.; Kobayashi, Y.; Nishibori, E.; Takata, M.; Sakata, M.; Shinohara, H. *Nature* **2000**, *408*, 426–427.

(5) Kobayashi, K.; Nagase, S. *Chem. Phys. Lett.* **2002**, *362*, 373–379.

(6) Takata, M.; Nishibori, E.; Sakata, M.; Wang, C.-R.; Shinohara, H. *Chem. Phys. Lett.* **2003**, *372*, 512–518.

(7) Stevenson, S.; Fowler, P. W.; Heine, T.; Duchamp, J. C.; Rice, G.; Glass, T.; Harich, K.; Hajdu, E.; Bible, R.; Dorn, H. C. *Nature* **2000**, *408*, 427–428.

(8) Olmstead, M. M.; Lee, H. M.; Duchamp, J. C.; Stevenson, S.; Marciu, D.; Dorn, H. C.; Balch, A. L. *Angew. Chem., Int. Ed.* **2003**, *42*, 900–903.

(9) Reveles, J. U.; Heine, T.; Köster, A. M. *J. Phys. Chem. A* **2005**, *109*, 7068–7072.

(10) Beavers, C. M.; Zuo, T.; Duchamp, J. C.; Harich, K.; Dorn, H. C.; Olmstead, M. M.; Balch, A. L. *J. Am. Chem. Soc.* **2006**, *128*, 11352–11353.

(11) Shi, Z.-Q.; Wu, X.; Wang, C.-R.; Lu, X.; Shinohara, H. *Angew. Chem., Int. Ed.* **2006**, *45*, 2107–2111.

(12) Yang, S.; Popov, A. A.; Dunsch, L. *Angew. Chem., Int. Ed.* **2007**, *46*, 1256–1259.

(13) Stevenson, S.; Burbank, P.; Harich, K.; Sun, Z.; Dorn, H. C.; van Loosdrecht, P. H. M.; deVries, M. S.; Salem, J. R.; Kiang, C.-H.; Johnson, R. D.; Bethune, D. S. *J. Phys. Chem. A* **1998**, *102*, 2833–2837.

(14) Kato, H.; Taninaka, A.; Sugai, T.; Shinohara, H. *J. Am. Chem. Soc.* **2003**, *125*, 7782–7783.

(15) Slanina, Z.; Chen, Z.; Schleyer, P. v. R.; Uhlik, F.; Lu, X.; Nagase, S. *J. Phys. Chem. A* **2006**, *110*, 2231–2234.

(16) Yamada, M.; Wakahara, T.; Lian, Y.; Tsuchiya, T.; Akasaka, T.; Waelchli, M.; Mizorogi, N.; Nagase, S.; Kadish, K. M. *J. Am. Chem. Soc.* **2006**, *128*, 1400–1401.

(17) Dunsch, L.; Bartl, A.; Georgi, P.; Kuran, P. *Synth. Met.* **2001**, *121*, 1113–1114.

(18) Frisch, M. J. GAUSSIAN 03, revision C. 01; Gaussian Inc.: Wallingford, CT, 2004.

(19) Cundari, T. R.; Stevens, W. J. *J. Chem. Phys.* **1993**, *98*, 5555–5565.

(20) Hariharan, P. C.; Pople, J. A. *Theor. Chim. Acta* **1973**, *28*, 213–222.

(21) Yamada, M.; Nakahodo, T.; Wakahara, T.; Tsuchiya, T.; Maeda, Y.; Akasaka, T.; Kako, M.; Yoza, K.; Horn, E.; Mizorogi, N.; Kobayashi, K.; Nagase, S. *J. Am. Chem. Soc.* **2005**, *127*, 14570–14571.

(22) Bleaney, B. *J. Magn. Reson.* **1972**, *8*, 91–100.

(23) Wang, X.; Zuo, T.; Olmstead, M. M.; Duchamp, J. C.; Glass, T. E.; Cromer, F.; Balch, A. L.; Dorn, H. C. *J. Am. Chem. Soc.* **2006**, *128*, 8884–8889.

(24) Iiduka, Y.; Ikenaga, O.; Sakuraba, A.; Wakahara, T.; Tsuchiya, T.; Maeda, Y.; Nakahodo, T.; Akasaka, T.; Kako, M.; Mizorogi, N.; Nagase, S. *J. Am. Chem. Soc.* **2005**, *127*, 9956–9957.

(25) Taninaka, A.; Kato, H.; Shino, K.; Sugai, T.; Heike, S.; Terada, Y.; Hashizume, T.; Shinohara, H. *e-J. Surf. Sci. Nanotechnol.* **2004**, *2*, 89–92.

JP804260D